Structure and interaction of point defects in transition-metal nitrides

L. Tsetseris,[1,2] N. Kalfagiannis,[1] S. Logothetidis,[1] and S. T. Pantelides[2,3]
[1]*Department of Physics, Aristotle University of Thessaloniki, GR-54124 Thessaloniki, Greece*
[2]*Department of Physics and Astronomy, Vanderbilt University, Nashville, Tennessee 37235, USA*
[3]*Oak Ridge National Laboratory, Oak Ridge, Tennessee 37831, USA*
(Received 2 October 2007; published 14 December 2007)

Transition-metal nitrides (TMNs) are used in a variety of applications because of their renowned hardness and stability. Departure from the nominal 1:1 stoichiometry is often observed for TMNs and, therefore, defects have a prevalent role on TMN physical properties. Here, we report the results of first-principles calculations on nitrogen and metal point defects in the prototype system of TiN and in HfN and ZrN. We find features which are common to all systems, while we unravel also key differences. In certain cases—for example, N interstitials in TiN—the interaction between defects is attractive and it favors the formation of defect complexes. Other defects, like N interstitials in HfN and ZrN, do not pair up. We also present results on the effect of point defects on the electronic properties of TiN. Finally, we discuss pertinent experimental data and the implications of our findings on the thermal stability of TMN films.

DOI: 10.1103/PhysRevB.76.224107 PACS number(s): 72.80.Ga, 61.72.Ji, 61.72.Bb, 68.60.Dv

I. INTRODUCTION

Transition-metal nitrides (TMNs) are hard refractory materials which crystallize normally in the rocksalt structure. The close-packed NaCl structure hampers the migration of species, with the result of excellent thermal stability against, for example, oxidation or self-diffusion.[1–5] For these reasons, TMNs are used widely as wear-resistant coatings in various applications and as diffusion barriers in electronic devices.[3,4,6] TiN, which is regarded as a prototype TMN system, and ZrN bear a goldlike appearance, and they are commonly used as protective overlayers in decorations. HfN is the most refractory of all TMNs with the highest melting point,[1] a property that makes it the material of choice for use in harsh environments. TMNs have recently attracted special attention as components of superhard materials.[7–9]

The structural, mechanical, electronic, and optical properties of bulk[10–12] and nanocrystalline TiN,[13,14] TiN surfaces,[15–20] and TiN-based alloys[12,21] and heterostructures[22,23] have been the focus of several experimental and theoretical studies. Several studies have also probed the effect of point defects on the electronic and mechanical properties of the host crystal. N vacancies, in particular, are regarded as the primary defects that control the composition ratio of substoichiometric transition-metal nitrides. Positron annihilation,[24] ellipsometry,[25] x-ray diffraction and photoemission spectra,[12,26,27] and electron energy loss spectra[28,29] have identified features in the electronic properties of TiN_x compounds consistent with the presence of N vacancies. First-principles calculations,[12,26–28] mostly using small supercells of ordered defect arrangements, have provided theoretical support for the relation between observed features and the presence of vacancies. Furthermore, a combination of experimental[27,30–32] and theoretical works[27,32,33] has provided a link between the elastic properties of the material and the existence of point defects. The details of the effect of impurities, such as vacancies and interstitials, on the properties of a host matrix, depend also on defect interactions, migration, and transformations. Theoretical studies of these effects require the use of large supercells and computational power and, to our knowledge, they are largely missing.

In this article, we use first-principles calculations to obtain the structure, stability, and interaction energies for the native defects of stoichiometric TiN, HfN, and ZrN. In a previous work[34] we discussed a limited number of results for N point defects in TiN with an emphasis on their role on thermal stability. Here, we extend the study of point imperfections to HfN and ZrN and we include metal as well as nitrogen defects. We find that N (V_N) and metal (V_{Ti}, V_{Hf}, V_{Zr}) vacancies cause a small outward relaxation of the crystal around the defect site. The interaction between neighboring N vacancies is weak in HfN and ZrN, while it is considerably repulsive in TiN. Metal vacancies also repel each other in TiN and HfN. The lowest energy arrangements of N interstitials I_N in TiN and HfN are those of split configurations with stretched N-N bonds aligned along certain crystal directions. The most stable I_N structure in ZrN is a tetrahedral configuration. In contrast to N vacancies, I_N pairs in TiN and HfN have a substantial binding energy and they are favored to form complexes in a herringbone pattern. Ti interstitials (I_{Ti}) are also favored in split configurations similar to those of I_N.

II. METHOD

The calculations were performed within density-functional theory (DFT), with a generalized-gradient corrected (GGA) exchange-correlation functional,[35] a plane-wave basis set with an energy cutoff (E_c) of 400 eV, and projector-augmented-wave (PAW) potentials,[36] as implemented in the VASP code.[37] We used PAW potentials with four valence electrons for Ti, Hf, and Zr, unless stated otherwise. Selected calculations with electronic configurations including semicore levels in the valence shell did not show significant deviations in the results and conclusions. The lattice constant was fixed at the experimental values of 4.2366 Å, 4.524 Å, and 4.574 Å for TiN,[10,13] HfN,[38,39] and

TABLE I. Binding (interaction) energies E^i for the most stable pairs of vicinal point defects in TiN, HfN, and ZrN. Positive (negative) numbers indicate repulsive (attractive) interaction. The reference energy is that of the corresponding lowest-energy structure of isolated point defects. Symbols used for geometry: $O(T)$ for octahedral (tetrahedral) site, S for split interstitial.

System	Defect	Geometry	E^i (eV)
TiN	V_N-V_N	*O-O*	0.23
TiN	V_N-V_N	*O-O*	0.19
TiN	I_N-I_N	*S-S*	−0.55
TiN	V_{Ti}-V_{Ti}	*O-O*	0.68
TiN	V_{Ti}-V_{Ti}	*O-O*	0.31
TiN	I_{Ti}-I_{Ti}	*S-S*	−0.31
HfN	V_N-V_N	*O-O*	−0.01
HfN	V_N-V_N	*O-O*	−0.10
HfN	I_N-I_N	*T-T*	0.34
HfN	V_{Hf}-V_{Hf}	*O-O*	0.62
HfN	V_{Hf}-V_{Hf}	*O-O*	0.24
HfN	I_{Hf}-I_{Hf}	*S-S*	−0.74
ZrN	V_N-V_N	*O-O*	0.07
ZrN	V_N-V_N	*O-O*	0.03
ZrN	I_N-I_N	*S-S*	0.29
ZrN	V_{Zr}-V_{Zr}	*O-O*	0.19
ZrN	V_{Zr}-V_{Zr}	*O-O*	−0.17
ZrN	I_{Zr}-I_{Zr}	*S-S*	0.18

ZrN,[40] respectively. The results we present below are based on $3\times3\times3$ supercells with 108 Ti and 108 N atoms when no defects are present. We tested the convergence of selected results with respect to supercell size using even larger $4\times4\times4$ supercells. We found that for the same cutoff energy (300 eV) and Γ-point sampling, the energy difference between tetrahedral and split I_N's in TiN, and between the most stable I_N-I_N pairs in TiN changes by less than 0.04 eV as we increase the supercell size from $3\times3\times3$ to $4\times4\times4$. We used a varying number of k points ($2\times2\times2$ and $3\times3\times3$ k grids) following the Mohnkorst-Pack scheme[41] for Brillouin zone sampling. In the following we report only the results based on $3\times3\times3$ k grids, unless stated otherwise. Previous studies[42] showed the importance of k-point sampling for the calculation of TiN elastic constants. In the present case, we find by comparing to selected calculations with finer grids ($4\times4\times4$ and $6\times6\times6$) that the results on relative stability of defects and defect binding energies are converged within about 0.1 eV. This accuracy is sufficient to decide on possible agglomeration and the role of the point defects discussed here on electronic properties and thermal stability of transition-metal nitrides. The interaction energies E^i between defects are presented in Table I. They were obtained by combining the energy of the host TMN, the energies of supercells with single defects A and B, and the energy of the supercell containing the defect complex AB:

$$E^i = E^{AB}_{\text{def}} + E_{\text{TMN}} - E^A_{\text{def}} - E^B_{\text{def}}. \tag{1}$$

Positive (negative) E^i's indicate repulsion (attraction) between defects.

TABLE II. Formation energies E^F of the most stable configurations of N point defects in TiN, HfN, and ZrN. E^F's are referenced with respect to defect-free structures and N_2 molecules in vacuum [Eq. (2)].

System	Defect	Geometry	E^F (eV)
TiN	V_N	Octahedral	2.41
TiN	I^b_N	Split $(10\bar{1})$ aligned	4.60
HfN	V_N	Octahedral	3.51
HfN	I^c_N	Tetrahedral	2.91
ZrN	V_N	Octahedral	3.15
ZrN	I^c_N	Tetrahedral	3.53

The formation energies E^F of the single N defects can be unambiguously referenced with respect to defect-free structures and N_2 molecules in vacuum. Their values are shown in Table II, and they are calculated with the formula

$$E^F = E_{\text{def}} + \frac{x}{2}E_{N_2} - E_{\text{TMN}}, \tag{2}$$

where E_{def} is the total energy of the defect supercell, E_{TMN} is the total energy of the host TMN supercell, E_{N_2} is the energy of a N_2 molecule in vacuum, and $x=1,-1$ for V_N and I_N defects, respectively.

III. RESULTS

We describe below in detail the results on the structure and possible pairing of vacancies and interstitials in TMNs. We first discuss N point defects and then metal-related imperfections. In each section, we start with the findings for TiN and then we present the results for HfN and ZrN.

A. N vacancies

A nitrogen vacancy induces a small outward relaxation[34] in the surrounding TiN matrix, as observed also in previous DFT studies.[33] The distance between neighboring Ti atoms and the N vacancy site changes[34] from the pristine value of 2.12 Å to 2.20 Å. The backbonds of these Ti atoms to Ti species of the second shell around the vacancy contract from 2.99 Å to 2.93 Å. Similar results have been obtained for relaxation around a C vacancy in TiC.[43,44] A small outward relaxation is also found around N vacancies in stoichiometric ZrN. The distance between vicinal Zr atoms and the V_N site changes slightly from 2.287 Å to 2.342 Å. Relaxation leads also to a small increase (from 2.262 Å to 2.304 Å) for the distance between Hf atoms and a V_N in HfN.

N vacancies are believed to be the defects that control the stoichiometry of transition-metal nitride films. The interaction between these defects is, therefore, crucial for the properties of these films. We studied this interaction for three N divacancy configurations: (i) both V_N's were placed in the same (110) chain, (ii) the V_N's were neighboring members of a (100) chain, and (iii) the two V_N's were placed in a distance of 7.9 Å with respect to each other. For the divacancies in TiN, interaction energies E^i's are slightly positive for neigh-

boring V_N's and they decrease to zero as the two defects move away from each other.[34] In cases (i) and (ii) the E^i's are 0.23 eV and 0.19 eV, respectively.

We further studied pairs of N vacancies in HfN and ZrN, and we obtained the interaction for V_N pair geometries as in cases (i) and (ii) above for TiN. The metal atoms next to N vacancies are displaced only very slightly (less than 0.1 Å) away for the ideal rocksalt positions. This feature is common to TiN, HfN, and ZrN. However, the V_N-V_N interaction is markedly repulsive in TiN, whereas it is weak in HfN and ZrN. The corresponding E^i's range between 0.00 eV and −0.10 eV. Therefore, a common feature for the three TMNs is the lack of a strong tendency for agglomeration of N vacancies.

In Ref. 34 we showed that the diffusion barriers for nitrogen vacancies in TiN and ZrN are very high. Their values are about 3.9 eV for both systems,[34] in agreement with pertinent experimental data.[1,3] As in previous studies that found good agreement between DFT-GGA barriers and experimental data,[34,45] we used the elastic band method[46] to calculate the vacancy migration barrier in HfN. For a $2\times2\times2$ k-point mesh, the minimum-energy pathway for V_N diffusion has an activation energy of 3.7 eV. Similar to TiN and ZrN, there are no hopping events for N vacancies in HfN, unless the sample is heated to extremely high temperatures. The suppression of V_N migration, in combination with the lack of strong attraction between N vacancies, underlies the stability of TMN films with nitrogen stoichiometry less than unity. Since V_N's stay practically idle for a wide temperature range, the rocksalt structure is retained against possible V_N clustering at surfaces, grain boundaries, or other extended defects and boundaries.

B. N interstitials

A second class of N point defects corresponds to N interstitials. There are a number of possibilities for the geometries of nitrogen interstitials in transition-metal nitrides. One possibility is an I_N in a tetrahedral position, as shown in Fig. 1(c) for a nitrogen interstitial (I_N^c) in ZrN. Other possible arrangements are split interstitials for which the extra N atom forms a stretched N-N bond with a N atom of the network. The stretched bond may be aligned along different directions. For example, Figs. 1(a) and 1(b) show two stable configurations (I_N^a and I_N^b) in ZrN with the N-N dimer pointing along the (111) and (10$\bar{1}$) directions. The results on the relative stability of split and tetrahedral N interstitial configurations are summarized in Table III. In the case of TiN,[34] I_N^b is the most stable nitrogen interstitial configuration. I_N^a is less stable by 0.20 eV, while the tetrahedral I_N^c arrangement is considerably less stable by 0.86 eV. The N-N dimer has a bond length of 1.33 Å for I_N^a and I_N^b in TiN.

N interstitials in HfN show similar structural features to I_N's in TiN, but their energy ordering is different. Tetrahedral arrangements are the most stable I_N configurations. The distance between the interstitial N atom and its vicinal Hf atoms is 1.98 Å. Split interstitials, with 1.39 Å stretched N-N bonds in the (111) and (10$\bar{1}$) directions, exist only as metastable configurations. The (111) and (10$\bar{1}$) structures are

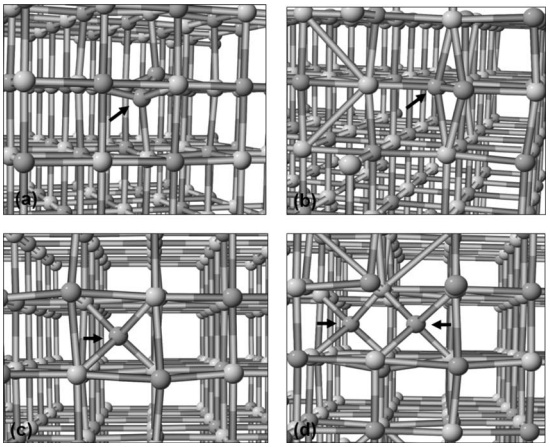

FIG. 1. N interstitials (I_N) in ZrN: (a) and (b) split interstitials with N-N stretched bonds aligned along (111) and (10$\bar{1}$) directions, (c) tetrahedral interstitial. Lowest-energy I_N configuration is (c). Structures (a) and (b) are 0.77 eV and 0.44 eV higher in energy, respectively. (d) Most stable pair of vicinal tetrahedral interstitials in ZrN. The energy of (d) is 0.37 eV higher than isolated tetrahedral interstitials. N interstitials are indicated with arrows (Zr, light gray; N, gray).

1.11 eV and 0.81 eV higher in energy than the tetrahedral I_N arrangement. I_N structures in ZrN are very similar to their HfN counterparts. The tetrahedral configuration is again the most stable, with the I_N atom at a distance of 2.02 Å from its neighboring Zr species. The split interstitials aligned along the (111) and (10$\bar{1}$) axes are higher in energy by 0.77 eV and 0.44 eV, respectively. Both split I_N's have N-N bonds stretched to 1.37 Å.

The most stable di-interstitial pair in TiN is a complex of two I_N^b's in neighboring sites.[34] Their binding energy is considerable and equal to 0.55 eV. The same number is obtained when the calculations employed a Ti PAW with the electrons of the 3s and 3p semicore levels in the valence shell (total Ti valency of 12). Other stable structures consist of I_N^b and I_N^a vicinal defects, or a I_N^a-I_N^a combination. Their binding energies are 0.41 eV and 0.18 eV, respectively.[34] The I_N-I_N in-

TABLE III. Relative stability of nitrogen interstitial point defects in TiN, HfN, and ZrN. The formation energy E^F of the most stable configuration is set to zero in each case.

System	Defect	Geometry	E^F (eV)
TiN	I_N^a	Split (111) aligned	0.20
TiN	I_N^b	Split (10$\bar{1}$) aligned	0.00
TiN	I_N^c	Tetrahedral	0.86
HfN	I_N^a	Split (111) aligned	1.11
HfN	I_N^b	Split (10$\bar{1}$) aligned	0.81
HfN	I_N^c	Tetrahedral	0.00
ZrN	I_N^a	Split (111) aligned	0.77
ZrN	I_N^b	Split (10$\bar{1}$) aligned	0.44
ZrN	I_N^c	Tetrahedral	0.00

teraction remains attractive (E^i of 0.44 eV) even in the case that an I_N^b and an I_N^b are located in a second-nearest-neighbor position.[34] Unlike the above stable I_N-I_N pairs, all the corresponding complexes with at least one of the N interstitials in a tetrahedral I_N^c configuration are unstable. In particular, the energy penalties for the formation of vicinal I_N^a-I_N^c, I_N^b-I_N^c, and I_N^c-I_N^c pairs are 0.94 eV, 0.78 eV, and 0.52 eV, respectively. We also considered the di-interstitial case with an N_2 molecule initially centered at the tetrahedral site of a TiN crystal. After relaxation, these two N atoms were stretched to a 1.48 Å distance and each of them came closer to a network N atom, at a distance of 1.36 Å. This relaxed configuration is, however, highly unstable by 1.39 eV, with respect to complete dissociation to a vicinal I_N^b-I_N^b pair.

Let us now discuss results on the stability of N interstitial complexes in HfN and ZrN. In contrast to TiN, no stable I_N-I_N pairs were found. The lowest-energy pair of vicinal interstitials in ZrN is a I_N^c-I_N^c complex of tetrahedral defects in the (110) direction. The configuration is shown in Fig. 1(d). The distance between the interstitial atoms is about 2.31 Å. However, the energy of this defect structure in ZrN (HfN) is higher by 0.37 eV (0.34 eV) compared to two isolated I_N's. This energy difference is the same when a Zr (Hf) PAW potential is used with the 4*p* (5*s* and 5*p*) electrons included in the valence shell. A small decrease in energy is obtained when the two I_N^c's move away from each other. Compared to isolated defects, ZrN (HfN) I_N^c-I_N^c pairs with a distance of 4.60 Å between two I_N's in the (100) direction are higher in energy by 0.10 eV (0.07 eV). Other interstitial structures discussed above for TiN are also unstable in the case of HfN and ZrN. The complete dissociation of I_N^a-I_N^b and I_N^a-I_N^b vicinal pairs in HfN (ZrN) results in the release of 1.05 eV (0.28 eV). Finally, the complex obtained after relaxation from an initial configuration with an interstitial N_2 molecule is highly unstable (by 1.47 eV and 0.70 eV) in both HfN and ZrN.

C. Metal vacancies

N vacancies and interstitials are believed to be the defects that dominate in TiN_x. Ti defects, however, are also expected to play a role and previous works[47] have suggested that they are responsible for some of the observed features. We examined the cases of Ti vacancies (V_{Ti}) and Ti interstitials (I_{Ti}) for TiN and similar metal defects for HfN and ZrN. As in the case of V_N, a small outward relaxation is induced in the surrounding TiN matrix around a V_{Ti}, and the distance of neighboring N atoms to the vacancy site changes from 2.12 Å to 2.17 Å. Similar relaxations are obtained around metal vacancy sites in HfN and ZrN. The N atoms surrounding a Hf (Zr) vacancy in HfN (ZrN) move away from the vacancy site by 0.073 Å (0.067 Å).

Neighboring V_{Ti}'s of the same (110) and (100) chain repel each other with E_i's of 0.68 eV and 0.31 eV. Ti vacancy clustering is therefore suppressed. Likewise, a repulsive interaction is found for pairs of vicinal metal vacancies in HfN. E_i's for (100) and (110) V_{Hf}-V_{Hf} pairs are 0.62 eV and 0.24 eV, respectively. The interaction between (100) vacancy pairs is repulsive in ZrN with an E^i of 0.19 eV. In contrast, the interaction is attractive (by 0.17 eV) for (110)-aligned divacancies in ZrN. We should note that, from all the quantities probed in this work, the interaction energies for vacancy pairs are the most sensitive to the calculational parameters. Specifically, for $2\times2\times2$ *k*-point sampling the (100) and (110) *V*-*V* interaction energies for HfN (ZrN) are 1.05 eV and 0.55 eV (1.12 eV and 0.67 eV), respectively. On the contrary, the same values with $2\times2\times2$ *k* mesh for TiN are 0.62 eV and 0.25 eV, indicating faster *k*-point convergence in this case.

TABLE IV. Relative stability of metal interstitial point defects in TiN, HfN, and ZrN. The formation energy E^F of the most stable configuration is set to zero in each case.

System	Defect	Geometry	E^F (eV)
TiN	I_{Ti}^a	Split (111) aligned	0.00
TiN	I_{Ti}^b	Split $(10\bar{1})$ aligned	0.22
TiN	I_{Ti}^c	Tetrahedral	0.16
HfN	I_{Hf}^a	Split (111) aligned	0.01
HfN	I_{Hf}^b	Split $(10\bar{1})$ aligned	0.00
HfN	I_{Hf}^c	Tetrahedral	1.56
ZrN	I_{Zr}^a	Split (111) aligned	0.00
ZrN	I_{Zr}^b	Split $(10\bar{1})$ aligned	0.82

D. Metal interstitials

The structural similarities between N and metal defects extend also to the case of interstitials. In the case of TiN, I_{Ti}'s exist in stable tetrahedral and split interstitial configurations with Ti-Ti dimers pointing along the (111) and $(10\bar{1})$ directions. The Ti-Ti bond lengths are 1.80 Å and 1.86 Å for the (111)- and $(10\bar{1})$-aligned dimers, respectively. In contrast to N interstitials, the lowest-energy I_{Ti} configuration is the split complex with the Ti-Ti dimer pointing in the (111) direction. The other two Ti interstitials, the tetrahedral I_{Ti} and the split I_{Ti} in the $(10\bar{1})$ direction, are higher in energy by 0.16 eV and 0.22 eV.

The results on the relative stability of split and tetrahedral metal interstitial configurations in TiN, HfN, and ZrN are summarized in Table IV. Split Hf interstitials along (111) and $10\bar{1}$ directions have almost the same formation energy. Tetrahedral Hf interstitials are significantly less stable, being 1.56 eV higher in energy. Zr interstitials, on the other hand, show different features. The (111) configuration is markedly lower in energy, by 0.82 eV, than the $(10\bar{1})$ structure. In the case of ZrN, an initial structure close to a tetrahedral interstitial configuration relaxed towards the most stable (111)-split arrangement.

Finally, we studied the stability of pairs of metal interstitials in the three TMNs. We considered vicinal split interstitials involving metal atoms in dimers along the (111) direction. For TiN and HfN a considerable binding energy is obtained with an E_i of 0.31 eV and 0.74 eV. Metal interstitials are, therefore, favored to form complexes in these two

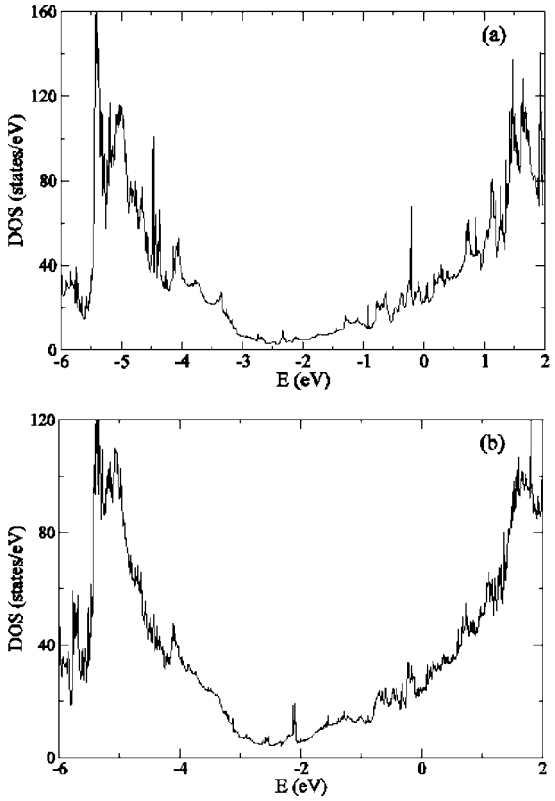

FIG. 2. Density of states for TiN with (a) no defects present and (b) with N interstitials in I_N^a split configurations. Results are based on supercells with 32 Ti atoms and 32 or 33 N atoms for the defect-free case. Zero of energy is set at the Fermi level.

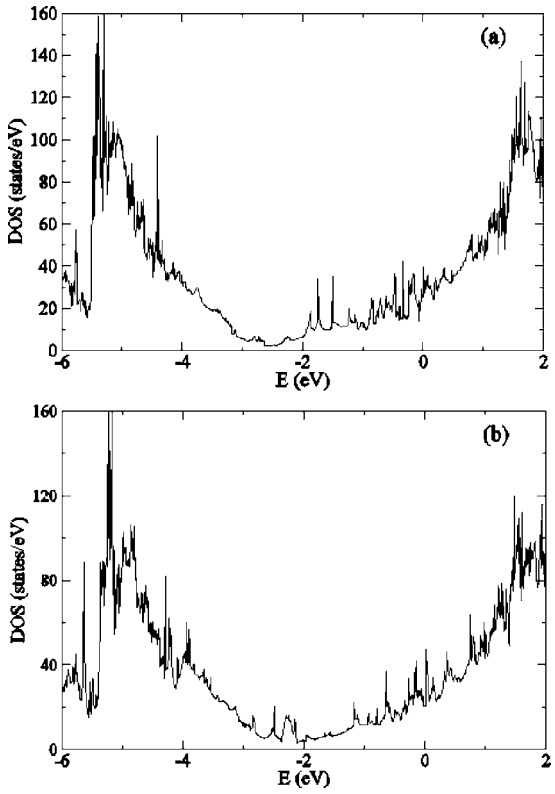

FIG. 3. Density of states for TiN with (a) an N vacancy and (b) a Ti vacancy. Results are based on supercells with 32 Ti atoms and 32 N atoms for the defect-free case. Zero of energy is set at the Fermi level.

systems. In contrast, the same defect pair in ZrN is not stable against dissociation and the energy of the complex is 0.18 eV higher compared to two isolated Zr interstitials.

E. Electronic properties

We now examine the effect of point imperfections on the electronic properties of TiN. Figure 2 shows the density of states (DOS) for TiN with no defects present. Figures 2 and 3 also show the density of states for TiN supercells with N interstitials, N and Ti vacancies. The results were obtained for $2\times2\times2$ supercells with 32 Ti and 32 N atoms in the defect-free case. $8\times8\times8$ or $16\times16\times16$ k-grids were used for Brillouin zone integrations with the tetrahedron method.[48] As shown in Fig. 2(a), the density of states of TiN ($16\times16\times16$ k-grid) shows a dip below the Fermi level (E_F). It is centered around 2 eV below E_F, in agreement with previous studies.[12] The two peaks surrounding the dip relate to bands of different symmetry. On the left, the N p bands dominate, while on the right the Ti d bands are the major component of the conduction band around the Fermi level.[10,12]

Our aim here is to investigate the effect of point imperfections on the electronic properties in the vicinity of the Fermi level. In Fig. 2(b) we give the DOS for TiN with split nitrogen interstitials in I_N^a configurations. We see that the presence of the defect can be identified with a distinct peak about 2.2 eV below the Fermi level. In contrast, the DOS for TiN with an I_N^b defect (not shown here) is very similar to the defect-free structure for this particular energy range and the above peak is missing. A relatively small change in geometry between I_N^b and I_N^b configurations has a discernible effect on DOS.

The presence of a nitrogen vacancy has a more pronounced effect on the DOS, as shown in Fig. 3(a) for a $12\times12\times12$ k grid. The right peak associated with the Ti states extends a shoulder in the dip region and peaks appear in the region of 1.8–2.0 eV below the Fermi level. V_N-related peaks in the same region were calculated by Tsujimoto *et al.*[28] using supercells of the same size as in the present case ($2\times2\times2$) and a linear-augmented plane-wave code. Other studies[12,33] have examined the effect of N vacancies on DOS, albeit on significantly higher vacancy concentrations and smaller supercells. There is, however, broad agreement between the present results and the studies for lower N stoichiometry x. For an x of 0.875, N vacancies[33] were shown to induce peaks in the same energy region as in Fig. 3(a).

In Fig. 3(b) we also show results on the DOS for a TiN supercell with a Ti vacancy ($8\times8\times8$ k grid). The defect causes extensive changes in the energy region around the Fermi level. Similar to V_N, the presence of a Ti vacancy relates to a distinct peak about 2.2 eV below E_F, slightly lower than the peaks related to V_N. A second smaller peak appears at about 2.5 eV below E_F. On the left side of these

two peaks, the part of DOS associated mostly with N *p* states rises at relatively higher energies compared to the ideal TiN case and to TiN with N vacancies.

IV. DISCUSSION

The existence of point defects is a very common feature in transition-metal nitrides. As a matter of fact, the experimental rule is that it is rather difficult to achieve the nominal stoichiometry. Moreover, the outstanding property of TMNs to retain the rocksalt structure for significant departures from 1:1 compositional ratio provides the option of defect engineering to tailor properties such as reflectivity, impurity permeability, and conductivity.

Although N vacancies are believed to be the most common defects in substoichiometric compounds, other point imperfections are present in samples prepared with different growth conditions. The choice of a particular substrate, method of growth, deposition rate, and ambient plays a role in the formation of defects. For example, TiN, HfN, and ZrN samples prepared with plasma vapor deposition show a propensity for both types (N and metal) of vacancies and interstitials.[1] Deposition by dc magnetron sputtering resulted in the preferential creation of Ti vacancies, as opposed to N interstitials.[14] A similar conclusion was reached in reactive arc deposition of TiN thin films.[47] Data from ellipsometry measurements on overstoichiometric TiN samples prepared by rf magnetron sputtering have been interpreted as evidence for N interstitials.[25]

The study of point defects has attracted considerable interest because it is known that these defects, along with extended imperfections such as dislocation loops and grain boundaries, control important physical properties. The gold-like appearance of TiN samples depends, for example, on the amount of N vacancies.[1,25] Another key property, the thermal stability, is generally believed to be affected by vacancies and interstitials.[3] Indeed, we showed recently using first-principles calculations[34] that the atomic-scale mechanisms on the stability, interactions and migration of point defects and their complexes can account for various changes of transition-metal nitrides after annealing at widely different temperatures.

Isolated nitrogen interstitials are the most mobile species in TiN and their migration has a relatively low activation energy of 1.28 eV.[34] As I_N's hop around they may encounter other such species. They then form stable interstitial pairs, as we discussed above. The migration of I_N pairs is not as facile as the diffusion of isolated I_N's, but it does represent the rate-limiting step at temperatures which are sufficiently high to activate the process. On the other hand, N interstitials in HfN and ZrN do not pair up. Consequently, even though isolated I_N's are expected to be relatively mobile in HfN and ZrN, no rate-limiting step associated with migration of interstitial complexes is expected. Finally, migration of nitrogen vacancies is largely suppressed in all TMNs, except for very high temperatures. As we stressed above, the lack of vacancy migration and clustering plays a key role for the preservation of the rocksalt structure for N stoichiometries much lower than unity.

Let us finally note that point defects are important also because they can play a role as trapping centers for other species. Inert gas atoms like argon or helium are typically expected to be present in samples grown under ion bombardment.[1,3] Other impurities, like carbon, oxygen,[10] and hydrogen, are often present after growth with chemical vapor deposition techniques. First-principles calculations[49] showed that hydrogen gets indeed trapped at N vacancy sites. More details on the interactions between native point defects and extrinsic species will be discussed elsewhere.[50]

V. SUMMARY

We have employed first-principles calculations to study the structural properties, stability, and interactions of point defects in TiN, HfN, and ZrN. Clustering of N vacancies is not favored in any of the three systems, especially because of very high diffusion barriers. The agglomeration tendency of interstitials, on the other hand, varies from one system to another. Interstitial pair formation is favored for N and Ti atoms in TiN and for Hf atoms in HfN. In contrast, the results indicate repulsive interactions for N interstitials in HfN and ZrN and Zr interstitials in ZrN. We investigated also the effect of N interstitials and N and Ti vacancies on the electronic properties of TiN. All these defects were shown to relate to distinct features, notably peaks of the density of states about 2 eV below the Fermi level.

ACKNOWLEDGMENTS

The authors acknowledge support by the William A. and Nancy F. McMinn Endowment at Vanderbilt University, AFOSR MURI Grant No. FA9550-05-1-0306, and Greek Secretariat for Research Technology Grant No. ΠΕΝΕΔ-03ΕΔ613. The calculations were performed at ORNL's Center for Computational Sciences.

[1] A. J. Perry, J. Vac. Sci. Technol. A **6**, 2140 (1988), and references therein.

[2] S. H. Jhi, J. Ihm, S. G. Louie, and M. L. Cohen, Nature (London) **399**, 132 (1999).

[3] L. Hultman, Vacuum **57**, 1 (2000), and references therein.

[4] F. Lévy, P. Hones, P. E. Schmid, R. Sanjinés, M. Diserens, and C. Wiemer, Surf. Coat. Technol. **120-121**, 284 (1999).

[5] I. Pollini, A. Mosser, and J. C. Parlebas, Phys. Rep. **355**, 1 (2001).

[6] D. J. Kim, Y. B. Jung, M. B. Lee, Y. H. Lee, J. H. Lee, and J. H. Lee, Thin Solid Films **372**, 276 (2000).

[7] J. Musil, Surf. Coat. Technol. **125**, 322 (2000).

[8] S. Hao, B. Delley, S. Veprek, and C. Stampfl, Phys. Rev. Lett. **97**, 086102 (2006).

[9] S. W. Wang, R. Gudipati, A. S. Rao, T. J. Bostelmann, and Y. G. Shen, Appl. Phys. Lett. **91**, 081916 (2007).
[10] H. Höchst, R. D. Bringans, P. Steiner, and T. Wolf, Phys. Rev. B **25**, 7183 (1982).
[11] Z. Dridi, B. Bouhafs, P. Ruterana, and H. Aourag, J. Phys.: Condens. Matter **14**, 10237 (2002).
[12] M. Guemmaz, G. Moraitis, A. Mosser, M. A. Khan, and J. C. Parlebas, J. Phys.: Condens. Matter **9**, 8453 (1997).
[13] J. Hu, Q. Lu, K. Tang, S. Yu, Y. Qian, G. Zhou, and X. Liu, J. Am. Ceram. Soc. **83**, 430 (2000).
[14] P. Patsalas and S. Logothetidis, J. Appl. Phys. **90**, 4725 (2001).
[15] P. A. P. Lindberg, L. I. Johansson, J. B. Lindström, and D. S. L. Law, Phys. Rev. B **36**, 939 (1987).
[16] B. W. Karr, D. G. Cahill, I. Petrov, and J. E. Greene, Phys. Rev. B **61**, 16137 (2000).
[17] S. Kodambaka, S. V. Khare, V. Petrova, A. Vailionis, I. Petrov, and J. E. Greene, Surf. Sci. **513**, 468 (2002).
[18] D. Gall, S. Kodambaka, M. A. Wall, I. Petrov, and J. E. Greene, J. Appl. Phys. **93**, 9086 (2003).
[19] C. S. Shin, S. Rudenja, D. Gall, N. Hellgren, T. Y. Lee, I. Petrov, and J. E. Greene, J. Appl. Phys. **95**, 356 (2004).
[20] P. Patsalas, C. Gravalidis, and S. Logothetidis, J. Appl. Phys. **96**, 6234 (2004).
[21] L. Calmels, C. Mirguet, and Y. Kihn, Phys. Rev. B **73**, 024207 (2006).
[22] P. Patsalas and S. Logothetidis, J. Appl. Phys. **93**, 989 (2003).
[23] N. Frangis, D. Papapetros, I. Tsiaoussis, and S. Logothetidis, Surf. Coat. Technol. **200**, 6201 (2006).
[24] J. P. Schaffer, A. J. Perry, and J. Brunne, J. Vac. Sci. Technol. A **10**, 193 (1992).
[25] P. E. Schmid, M. S. Sunga, and F. Lévy, J. Vac. Sci. Technol. A **16**, 2870 (1998).
[26] M. Guemmaz, A. Mosser, and J. C. Parlebas, J. Electron Spectrosc. Relat. Phenom. **107**, 91 (2000).
[27] M. Guemmaz, A. Mosser, R. Ahuja, and J. C. Parlebas, Int. J. Inorg. Mater. **3**, 1319 (2001).
[28] M. Tsujimoto, H. Kurata, T. Nemoto, S. Isoda, S. Terada, and K. Kaji, J. Electron Spectrosc. Relat. Phenom. **143**, 159 (2005).
[29] C. Mirguet, L. Calmels, and Y. Kihn, Micron **37**, 442 (2006).
[30] T. Lee, K. Ohmori, C. S. Shin, D. G. Cahill, I. Petrov, and J. E. Greene, Phys. Rev. B **71**, 144106 (2005).
[31] J. H. Kang and K. J. Kim, J. Appl. Phys. **86**, 346 (1999).
[32] C. S. Shin, D. Gall, N. Hellgren, J. Patscheider, I. Petrov, and J. E. Greene, J. Appl. Phys. **93**, 6025 (2003).
[33] S. H. Jhi, S. G. Louie, M. L. Cohen, and J. Ihm, Phys. Rev. Lett. **86**, 3348 (2001).
[34] L. Tsetseris, N. Kalfagiannis, S. Logothetidis, and S. T. Pantelides, Phys. Rev. Lett. **99**, 125503 (2007).
[35] J. P. Perdew and Y. Wang, Phys. Rev. B **45**, 13244 (1992).
[36] P. E. Blöchl, Phys. Rev. B **50**, 17953 (1994).
[37] G. Kresse and D. Joubert, Phys. Rev. B **59**, 1758 (1999).
[38] W. H. B. Hoondert, B. J. Thijsse, and A. van de Beukel, Surf. Coat. Technol. **66**, 472 (1994).
[39] H. S. Seo, T. Y. Lee, J. G. Wen, I. Petrov, J. E. Greene, and D. Gall, J. Appl. Phys. **96**, 878 (2004).
[40] J. Pflüger, J. Fink, W. Weber, K. P. Bohnen, and G. Crecelius, Phys. Rev. B **31**, 1244 (1985).
[41] D. J. Chadi and M. L. Cohen, Phys. Rev. B **8**, 5747 (1973).
[42] S. Nagao, K. Nordlund, and R. Nowak, Phys. Rev. B **73**, 144113 (2006).
[43] H. W. Hugosson, P. Korzhavyi, U. Jansson, B. Johansson, and O. Eriksson, Phys. Rev. B **63**, 165116 (2001).
[44] L. Tsetseris and S. T. Pantelides (unpublished).
[45] L. Tsetseris and S. T. Pantelides, Appl. Phys. Lett. **86**, 112107 (2005); Phys. Rev. B **74**, 113301 (2006).
[46] G. Mills, H. Jónsson, and G. K. Schenter, Surf. Sci. **324**, 305 (1995).
[47] G. B. Smith, P. D. Swift, and A. Bendavid, Appl. Phys. Lett. **75**, 630 (1999).
[48] O. Jepsen and O. K. Andersen, Solid State Commun. **9**, 1763 (1971).
[49] L. Tsetseris, D. M. Fleetwood, R. D. Schrimpf, X. J. Zhou, I. G. Batyrev, and S. T. Pantelides, Microelectron. Eng. **84**, 2344 (2007).
[50] L. Tsetseris, N. Kalfagiannis, S. Logothetidis, and S. T. Pantelides (unpublished).